Influence of fine content on the behavior of sandy soils undergoing artificial freezing in triaxial conditions

Canadian Geotechnical Journal

Research Article

Influence of fine content on the behavior of sandy soils undergoing artificial freezing in triaxial conditions

Giulia La Porta[a], **Francesca Casini**[b], **and Marina Pirulli**[a]

[a]Department of Structural, Geotechnical and Building Engineering, Politecnico di Torino, Turin, Italy; [b]Department of Civil Engineering and Computer Science Engineering, University of Rome Tor Vergata, Rome, Italy

Corresponding author: **Giulia La Porta** (email: giulia.laporta@polito.it)

Abstract

Artificial ground freezing (AGF) is used to stabilize loose soils and fractured rocks during tunnel and shaft excavation, ensuring temporary ground stabilization and groundwater control. It is particularly relevant for intermediate soils, where the influence of granulometry on freezing is crucial for effective design. However, existing studies often focus on site-specific materials, limiting broader applicability. This research investigates how fine content influences the freezing behavior of intermediate soils. Sandy soils with varying kaolin content (0% to 15%) are tested under different confining pressures representative of AGF applications. A modified triaxial apparatus simulated field conditions, applying radial thermal loading to replicate freezing around a pipe. Results demonstrated a pronounced dependence on kaolin content. Samples with 15% kaolin exhibited significant swelling, whereas soils with lower kaolin content were classified as non-frost-susceptible. Swelling was mitigated by increasing confining pressure. Water drainage was observed during the freezing process, governed by two mechanisms: (1) the expulsion of liquid water from the freezing front as water turned into ice and (2) cryogenic suction, which drew water toward the freezing front. These findings contribute to a more generalized and quantitative understanding of soil behavior with varying fine content under freezing conditions, facilitating the optimization of AGF applications.

Key words: artificial ground freezing, experimental tests, intermediate soils, fine content, freezing process, thermo-hydro-mechanical behavior

Résumé

Le gel artificiel du sol (AGF) est utilisé pour stabiliser les sols meubles et les roches fracturées lors de l'excavation de tunnels et de puits, assurant une stabilisation temporaire du sol et un contrôle des eaux souterraines. Il est particulièrement pertinent pour les sols intermédiaires, où l'influence de la granulométrie sur le gel est cruciale pour une conception efficace. Cependant, les études existantes se concentrent souvent sur des matériaux spécifiques au site, limitant ainsi leur applicabilité plus large. Cette recherche examine comment la teneur en fines influence le comportement de gel des sols intermédiaires. Les sols sableux avec une teneur variable en kaolin (0 % à 15 %) sont testés sous différentes pressions de confinement représentatives des applications AGF. Un appareil triaxial modifié a simulé les conditions de terrain, en appliquant un chargement thermique radial pour reproduire le gel autour d'un tuyau. Les résultats ont démontré une dépendance marquée à la teneur en kaolin. Les échantillons contenant 15 % de kaolin ont montré un gonflement significatif, tandis que les sols à faible teneur en kaolin ont été classés comme non sensibles au gel. L'enflure a été atténuée par une pression de confinement accrue. Le drainage de l'eau a été observé lors du processus de congélation, régi par deux mécanismes : (1) l'expulsion de l'eau liquide du front de congélation lorsque l'eau se transforme en glace, et (2) la succion cryogénique, qui attire l'eau vers le front de congélation. Ces résultats contribuent à une compréhension plus généralisée et quantitative du comportement du sol avec des teneurs fines variables en conditions de congélation, facilitant l'optimisation des applications AGF.

Mots-clés : congélation artificielle du sol, essais expérimentaux, sols intermédiaires, teneur en fines, procédé de congélation, comportement thermo-hydro-mécanique

1. Introduction

Artificial ground freezing (AGF) is a temporary ground stabilization technique used to control groundwater infiltration in excavations until a permanent structural lining is installed (Andersland and Ladanyi 2003). AGF consists in embedding freezing pipes within the excavation zone and circulating a refrigerant fluid through them to reduce the temperature of the surrounding soil below the freezing point of water. This process forms a frozen barrier that effectively restricts groundwater flow. Various refrigerants may be used, such

as liquid brine (recirculated), liquid nitrogen (which evaporates post-usage), or carbon dioxide. The latter, a more recent approach, offers several benefits, such as lower costs, improved worker safety, and simplified installation procedures (Shuplik and Nikolaev 2019).

AGF improves the mechanical properties of the soil, including strength and stiffness, while ensuring the impermeability of the frozen soil mass. However, the freezing process involves complex thermal, hydraulic, and mechanical interactions within soil pores, where temperature-induced phase changes affect the hydraulic regimes and may induce mechanical deformation. Hydraulic and mechanical conditions, in turn, influence thermal processes through advection and changes in ice and water content (Gens 2010). The coexistence of ice and water in soil pores below the bulk freezing point is due to curvature-induced and interfacial free energy effects within the soil–water–ice system (Wettlaufer and Worster 2006). The soil freezing retention curves (SFRCs) quantify the unfrozen water content relative to temperature, with grain size distribution being a significant influencing factor (Vu et al. 2022).

AGF is often applied in soils with intermediate and well-graded granulometry (e.g., Haβ and Schäfers 2005; Viggiani and De Sanctis 2009; Viggiani and Casini 2015; Hu et al. 2018; Shuplik and Nikolaev 2019; Casini et al. 2023; Guida et al. 2025). Freezing can result in frost heave, notably influenced by grain size distribution (Carter and Bentley 2016). The phenomenon of cryogenic suction – the process of drawing water through a soil matrix toward a freezing domain – is particularly significant in intermediate soils. They are recognized as the most frost-susceptible ones, due to the soil suction at the freezing front and a sufficiently high permeability to allow water migration (Carter and Bentley 2016). The fine content in soils can heighten suction due to increased meniscus curvature and residual unfrozen water content in pores (Vu et al. 2022), especially in the presence of non-active clays. This phenomenon increases heave during freezing (e.g., Konrad 2005; Li et al. 2017; Gao et al. 2018; Long et al. 2018; Wang et al. 2022), as the larger surface area of fine particles elevates surface energy, thereby promoting cryogenic suction. Moreover, the increase in unfrozen water content associated with higher fine contents enhances water migration along preferential pathways. Existing studies have analyzed coarse–fine soil mixtures at ambient temperature (e.g., Lade et al. 1998; Yang et al. 2006; Reiffsteck et al. 2007), including sand–clay compositions (Yin et al. 2021), but different issues remain open on their behavior upon freezing. In this direction, Vu et al. (2022) demonstrated that the fine content within sandy matrices significantly influences residual unfrozen water content, soil permeability, freezing temperature, and thermal conductivity.

Soil deformation during freezing arises from cryogenic suction toward the freezing front and the expansion of water upon freezing, which repels remaining liquid water and affects drainage and deformation dynamics. As to the experimental approaches to analyze soil strain upon freezing, most of the existing studies use one-dimensional (1D) experiments (e.g., Taber 1930; Long et al. 2018; Wang et al. 2022), even though triaxial testing may better simulate in situ AGF conditions. Furthermore, the method used to freeze soil samples still remains the main issue. Typically, samples are frozen using a freezer or directly within mechanical devices, with freezing initiated from either the top, bottom or radial edges of the sample (e.g., Arenson et al. 2004; Lai et al. 2014; Esmaeili-Falak et al. 2018; Xu et al. 2019; Cai et al. 2019). In many cases, any applied confining pressure is imposed only after freezing, disregarding the impact of confining pressure during the freezing process (Arenson and Springman 2005; Yamamoto and Springman 2014). This approach can produce unrealistic stress conditions within the soil and ice phases, deviating from those found in field applications, as observed by Nishimura and Wang (2019) in studies on clays. Only a few studies apply confining pressure prior to freezing, such as those by Wang et al. (2017) and Chen et al. (2020). In these studies, freezing is achieved by cooling the cell fluid, causing the sample to freeze progressively from the exterior toward its core. Consequently, a frozen layer, or frozen crown, rapidly forms along the exterior wall of the sample, restricting the soil ability to drain water and deform as freezing progresses. In contrast, during AGF applications, soil surrounding the freezing pipe generally remains free to drain and deform throughout the freezing process.

To address the aforementioned issues and accurately replicate in situ conditions, an experimental campaign is conducted using the modified triaxial apparatus *FROZEN* described by Bartoli et al. (2020). The apparatus features a central copper tube that applies the thermal load from within the sample, inducing freezing from the inside outward. This setup allows the soil to freely deform and facilitates both water in- and outflow during the advancement of the freezing front. Additionally, a consolidation step is performed prior to freezing, ensuring stress conditions that closely resemble those found in field applications.

This study aims to investigate the freezing behavior of intermediate soils. Specifically, gap-graded soils with a coarse matrix are analyzed by incrementally adding kaolin to a sandy matrix, resulting in a fine content ranging between 0% and 15%. The thermohydromechanical behavior of these mixtures is evaluated under three distinct confining pressures. Effective confinement stresses of 50, 200, and 800 kPa were selected to represent stress states typically encountered at shallow and deeper depths in AGF applications. This range allows for investigating the influence of different overburden conditions on the mechanical and hydraulic response of the mixtures during the freezing process.

2. Description of the experimental campaign

The experimental campaign was aimed to investigate the behavior of gap-graded soils during freezing and to assess their strength in a frozen state relative to their natural, unfrozen condition. For this purpose, testing was conducted using two distinct devices: a standard triaxial apparatus operating at ambient temperature, described by Lo Presti et al. (1994), and a modified triaxial apparatus for freezing tests, designated as *FROZEN* and described in Section 2.2.

Table 1. Summary and nomenclature of the tests conducted.

Sand (%)	Effective confining pressure (kPa) 50	200	800	Kaolin (%)
100	S100K0-50	S100K0-200	S100K0-800	0
92.5	S92.5K7.5-50	S92.5K7.5-200	S92.5K7.5-800	7.5
85	S85K15-50	S85K15-200	S85K15-800	15

Table 2. Physical properties of Fontainebleau sand (El Dine et al. 2010) and Speswhite kaolin (Boussaid 2005).

Fontainebleau sand		Speswhite kaolin	
Uniformity coefficient, C_U	1.52	Liquid limit, LL (%)	55
Medium grain size, d_{50} (mm)	0.21	Plastic limit, PL (%)	30
Specific gravity of solid grains, G_s	2.65	Plasticity Index, PI (%)	25
Minimum void ratio, e_{min}	0.54	Specific gravity of solid grains, G_s	2.65
Maximum void ratio, e_{max}	0.94		

Three sand–kaolin mixtures were tested, consisting of a sandy matrix with incremental kaolin contents of 0%, 7.5%, and 15%. Sample preparation followed established procedures described in detail in Section 2.1.

The samples utilized in the standard triaxial device had a diameter of 70 mm and a height of 140 mm, whereas the soil samples employed in *FROZEN* measured 100 mm in diameter and 200 mm in height. Although the testing protocol was largely consistent across both devices, minor procedural adjustments were required during the saturation phase due to differences in the pressure transducers' ability to handle low pressures. Consequently, saturation was conducted under an effective confining stress of 30 kPa in the *FROZEN* apparatus and 15 kPa in the standard triaxial device. Besides a complete analysis of the soil behavior, this study addresses the comparability of the results from the two setups.

Following saturation, specimens were consolidated under three consolidation pressures: 50, 200, and 800 kPa. In the standard triaxial apparatus, the shear phase initiated immediately after the consolidation phase. In contrast, within the *FROZEN* apparatus, samples underwent consolidation, followed by freezing until thermal equilibrium was reached, and subsequently the shear phase was conducted. The latter is performed through standard axial compression; however, this final stage is outside the scope of the present study.

For clarity, a standardized nomenclature will be used to refer to test conditions, used for both the nine tests conducted at ambient temperature (with the standard triaxial device) and the nine under freezing conditions (with *FROZEN*). S%K% represents the sand (S) and kaolin (K) mass percentages, followed by the value of the applied effective confining pressure. For example, S92.5K7.5-50 indicates a mixture with 7.5% kaolin, tested under an effective confining pressure of 50 kPa (Table 1).

2.1. Characteristics of the soil mixtures under investigation

The coarse material used in the experimental tests is Fontainebleau sand, a french sand characterized by a nearly uniform grain-size distribution, with grain diameters ranging from 100 to 400 μm.

Fig. 1. Grain-size distribution curves for the tested pure Fontainebleau sand, pure Speswhite kaolin, and their mixtures.

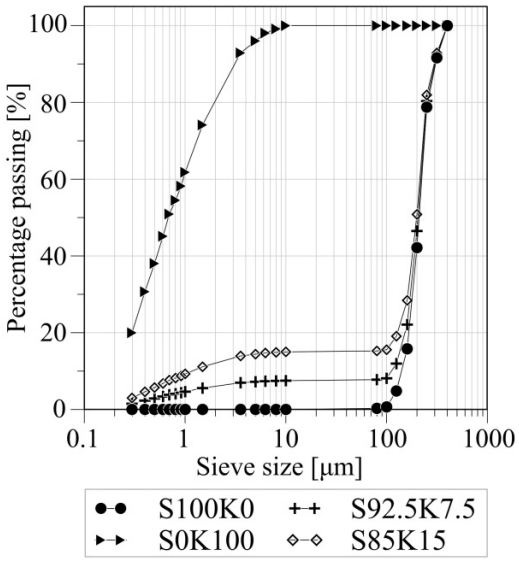

For the purposes of this experimental campaign, Fontainebleau sand is mixed with Speswhite kaolin, a non-active clay known for its relatively high permeability compared to other clays, typically ranging between 10^{-5} and 10^{-6} mm/s (Al-Tabbaa and Wood 1987).

The physical properties of the selected sand and kaolin and the grain-size distributions of the individual materials and their mixtures are given in Table 2 and Fig. 1, respectively.

The preparation procedure begins with mixing of sand and distilled water using an electric mixer. Kaolin is then gradually added while mixing is continued. Once all kaolin has been incorporated, the mixture is stirred for an additional 10 min to ensure homogeneity (Kenney et al. 1992). The

Table 3. Sum-up of the preparation method and target initial conditions of the mixtures.

Material	Preparation method		Target initial conditions	
Kaolin content (%)	STANDARD	*FROZEN*	w (%)	e (−)
0, 7.5, 15	Compaction by layers		7.2	0.74

Fig. 2. (*a*) Layout of *FROZEN*. (*b*) Positioning of thermocouples inside (triangles) and outside (circles) the sample.

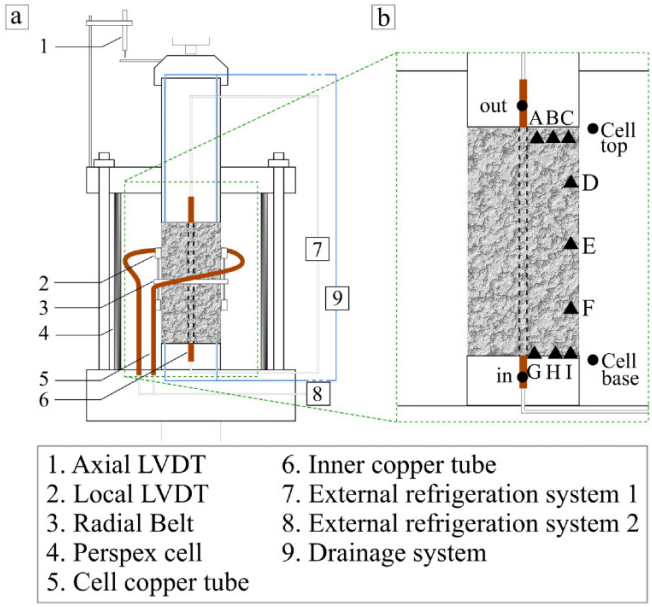

prepared mixture is subsequently sealed in an airtight bag for approximately 24 h to allow for uniform water distribution throughout the solid mass. Following this period, the sample is compacted in layers within a mold. The surface of each intermediate layer is roughened to prevent the formation of separation planes between successive layers.

All mixtures were prepared with a targeted initial water content and porosity to ensure comparable initial conditions. Specifically, an initial water content of 7.2% – corresponding to the optimum moisture content of pure sand (Ferrigno 2019) – and a porosity of 0.43 (equivalent to a void ratio of 0.74) were set as target values across all samples. This target porosity refers to the condition immediately after sample preparation, i.e., following the initial compaction phase, and prior to saturation. This approach was adopted to isolate and analyze the effects of varying fine content while preserving consistency in the initial conditions.

Table 3 summarizes the sample preparation methods and the theoretical initial conditions adopted for the tests.

2.2. The *FROZEN* apparatus

Figure 2*a* shows the modified triaxial apparatus used in the experimental campaign, referred to as *FROZEN* (Bartoli et al. 2020)—Italian Patent No. IT102017000138835. This apparatus is specifically designed to simulate the AGF process that occurs in situ around a freezing pipe. It comprises three main components: a mechanical press, a triaxial cell, and a refrigeration system. The first two are standard components, while the last one is uniquely designed in two parts to provide both internal (system 1 in Fig. 2*a*) and external (system 2 in Fig. 2*a*) cooling of the sample.

The internal refrigeration is achieved through a copper tube running longitudinally through the center of the soil sample, creating a radial thermal gradient across it. External cooling is provided by using a second copper tube that surrounds the sample, allowing precise temperature regulation within the cell. Ethylene glycol circulates through both refrigeration systems, serving as the coolant.

During the freezing process from the inner copper tube toward the outside of the sample, the specimen is allowed to deform freely, with water drainage permitted until the advancing freezing front reaches the drainage system.

Volumetric strains are monitored using a radial belt, local linear variable displacement transducers (LVDT) and an external axial LVDT placed at the top cap of the triaxial cell (Fig. 2*a*).

The volumetric strain is defined by the relation $\epsilon_v = \epsilon_a + 2\epsilon_r$.

The axial strain ϵ_a is calculated as $\epsilon_a = -\Delta H/H_0$, where H_0 and H are the initial and current height of the sample, respectively, with $\Delta H = H - H_0$.

Radial displacements are measured by the radial belt located at the mid-height of the sample. In this work, radial displacements are assumed to be constant along the sample height. The radial strain is therefore calculated as $\epsilon_r = -\Delta R/R_0$, where R_0 and R are the initial and current radii of the sample, respectively, with $\Delta R = R - R_0$.

The current void ratio e is determined as $e = e_0 - \epsilon_v(1 + e_0)$, where e_0 is the initial void ratio. The change in void ratio Δe is thus given by $\Delta e = \epsilon_v(1 + e_0)$.

For a water-saturated system undergoing freezing, Δe is expressed as follows:

$$\Delta e = \frac{\Delta V_v}{V_s} = \frac{\Delta V_w + \Delta V_{\text{ice}}}{V_s} = \Delta e_w + \Delta e_{\text{ice}} \quad (1)$$

where V_v, V_s, V_w, and V_{ice} denote the volumes of voids, solid, water-filled voids, and ice-filled voids, respectively. $\Delta e_w = \Delta V_w/V_s$ represents the variation in water ratio, while $\Delta e_{\text{ice}} = \Delta V_{\text{ice}}/V_s$ is the variation in ice ratio relative to the onset of the freezing process. ΔV_v is obtained from experimental measurements of ΔV, and ΔV_w is measured using the drainage system. Thus, $\Delta V_{\text{ice}} = \Delta V_v - \Delta V_w$ is analytically derived.

Δe is positive during swelling, while Δe_w is positive when water flows into the sample.

In this work, the frost-heaving ratio, defined in the literature under 1D oedometric conditions as $\eta_{1D} = \Delta H/H_0 \times 100$ during freezing (e.g., Long et al. 2018; Wang et al. 2022), is

Fig. 3. (*a*) Steps of the experimental procedure. (*b*) Example of measured temperature distribution during the freezing phase, for the test S100K0-200. For reference, the thermocouple layout is provided in Fig. 2*b*.

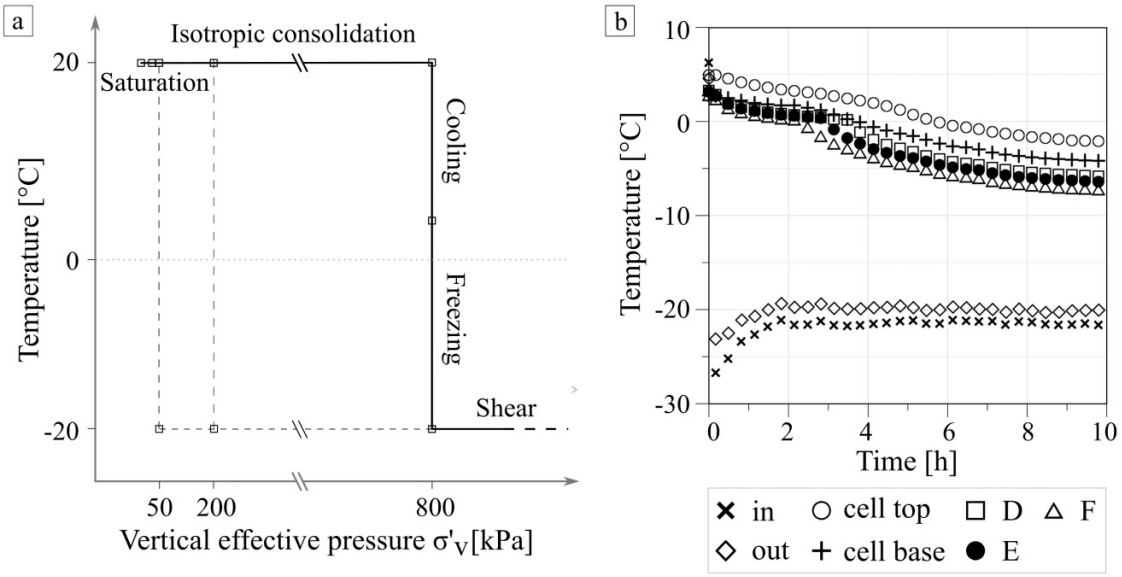

extended to three-dimensional (3D) conditions as follows:

$$\eta = \frac{\Delta V}{V_0} \times 100 \quad (2)$$

where $\Delta V \equiv \Delta V_v$.

According to the existing literature, a threshold of 1% is recommended as a criterion for evaluating the frost susceptibility of soils (Konrad 2008).

Temperature monitoring is conducted using thermocouples placed along the height of the sample, as illustrated in Fig. 2*b*. Thermocouples located inside the sample are represented by triangles, while those positioned outside are indicated by circles. Inside the sample, thermocouples are distributed at both the base and top along the radius (Fig. 2*b*: A, B, C, G, H, I), and every 50 mm along the vertical external edge (Fig. 2*b*: D, E, F). Additionally, two thermocouples monitor the temperature of the fluid circulating inside the inner tube (labeled "in" and "out" in Fig. 2*b*), while two others are placed within the cell fluid (labeled "cell base" and "cell top").

2.3. Experimental procedure

The experimental procedure is outlined in Fig. 3*a*. It consists of three main stages: an initial saturation phase of the specimen, followed by isotropic consolidation, and finally a freezing phase.

Saturation is conducted in accordance with standard guidelines (ASTM 2020). After flushing the sample first with carbon dioxide and then with de-aerated water, confining pressure is gradually increased while maintaining constant effective stress, until full saturation is achieved.

Following saturation, samples are consolidated under three different effective consolidation pressures: 50, 200, and 800 kPa. During consolidation, each specimen is cooled to approximately 5 °C via a coolant circulating through the outer copper tube (Fig. 2*a*). Once consolidation is complete, the freezing phase is initiated by lowering the temperature of refrigerant in the inner copper tube (Fig. 2*a*) to approximately −20 °C, while the temperature in the outer copper tube is kept nearly constant.

As the freezing progresses, the temperature of the cell fluid is also lowered to subzero levels to ensure that the entire sample reaches a fully frozen state. To prevent freezing on the sample's outer surface as the freezing front propagates outward from the inner copper tube, the cell fluid temperature (measured at "cell base" and "cell top") is kept at a higher level than the temperatures measured at points D, E, and F (thermocouples positioned along the sample height). This temperature control is achieved using the external refrigeration system (system 2 in Fig. 2*a*), as illustrated in Fig. 3*b*. The freezing phase typically lasts around 10 h.

At the end of this phase, the specimens achieve a steady-state condition characterized by a stable thermal gradient. The steady-state cell fluid temperature ("cell base" and "cell top" in Fig. 2*b*) is higher than that of the coolant in the inner tube ("in" and "out"). A vertical temperature gradient of approximately 2 °C is also observed between measurements at the bottom and top of the sample ("cell base" vs. "cell top" and "in" vs. "out"), likely influenced by factors as coolant viscosity, thermal exchange with the soil, and system heat dissipation. Figure 3*b* illustrates the typical temperature distribution within the samples during freezing, highlighting the observed thermal gradient.

3. Observations from experimental testing

A total of nine tests were conducted using the standard triaxial apparatus (Lo Presti et al. 1994) to understand the mechanical behavior of the soil mixtures under saturated

Fig. 4. (*a*) Proctor curves of the S100K0, S90K10, and S80K20, and initial conditions of the tested mixtures. (*b*) Measured potential collapse of samples under two effective pressures applied during saturation: 30 kPa in the *FROZEN* apparatus and 15 kPa in the standard apparatus.

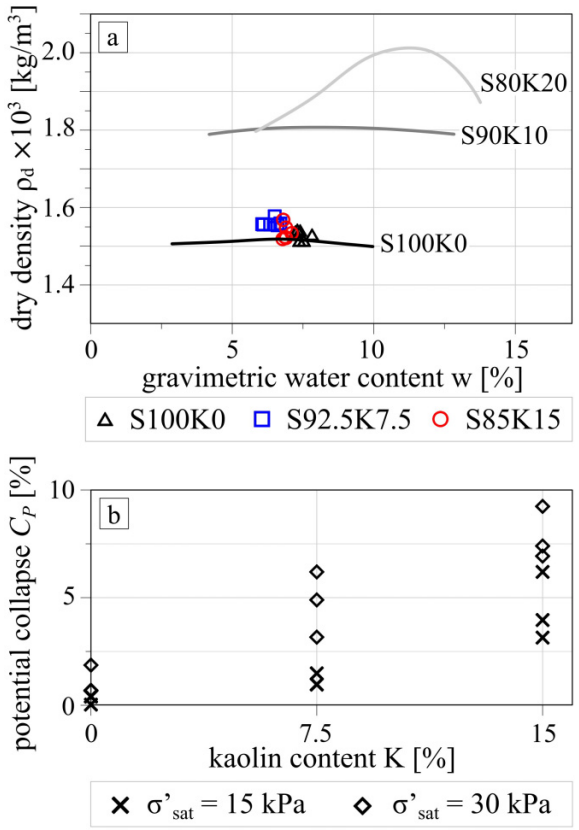

and unfrozen conditions. These results are compared with the data from the nine additional tests performed on soils subjected to freezing conditions using the *FROZEN* apparatus. While acknowledging the differences in geometry and boundary conditions (BCs) between the two setups, the room-temperature tests still provide a valuable reference for assessing soil response under standard conditions, serving as a baseline for comparison with the frozen tests. A subset of these tests was repeated to assess the consistency and reliability of the results.

Figure 4*a* illustrates the initial conditions of the tested samples plotted on the Proctor plane, indicating that the analyzed mixtures fall on the dry side of their respective Proctor curve.

From a microstructural perspective, the sand–clay mixtures (Section 2.1) compacted at the dry side exhibit a bimodal pore size distribution (PSD) (Vu 2022). This distribution is characterized by the presence of micropores (intra-aggregate porosity), which increase with a higher fine content, in addition to macropores (inter-aggregate porosity) (e.g., Casini et al. 2012; Vu et al. 2022). Upon wetting, soils with a bimodal PSD exhibit compaction, which primarily affects the macroporosity (e.g., Alonso et al. 2013; Romero 2013; Della Vecchia et al. 2015).

Fig. 5. Comparison of the void ratio measured in samples tested using the standard apparatus (*S*) and *FROZEN* (*F*), showing values at three stages: after preparation (initial), post-saturation, and post-consolidation.

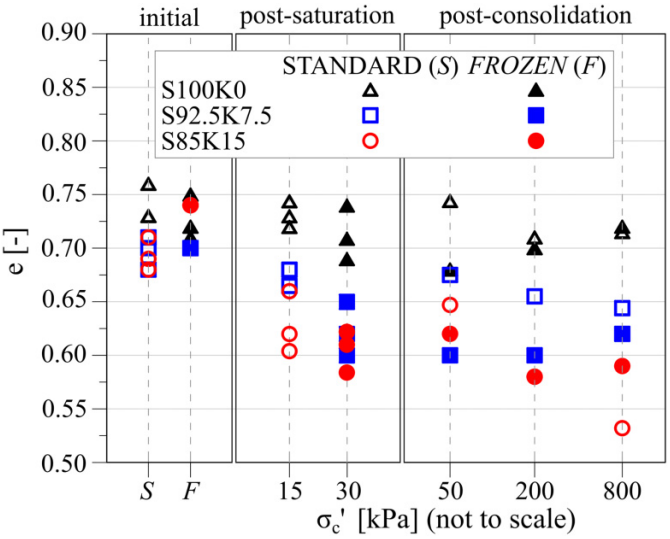

In the following, the results of the saturation, consolidation, and freezing phases are analyzed. Finally, a comprehensive discussion of the experimental result is provided.

3.1. Saturation and consolidation phases

As mentioned in Section 2, samples have been saturated under an effective confining stress of 30 kPa in the *FROZEN* apparatus and 15 kPa in the standard triaxial device. This resulted in different responses of the mixtures during the wetting process. To investigate this aspect, the potential collapse (C_P) is used. It quantifies the reduction in void ratio during saturation, which is the phase that predominantly influences the void ratio changes, and is defined as

$$C_P = \frac{\Delta e_{sat}}{1 + e_{0,sat}} \quad (3)$$

where Δe_{sat} represents the change in void ratio during saturation, and $e_{0,sat}$ is the void ratio prior to saturation (i.e., after sample packaging). Figure 4*b* illustrates the C_P values for different kaolin contents: a greater degree of collapse is observed with increasing applied effective stress. Moreover, the fine content significantly affects the degree of void collapse during saturation.

During consolidation, the mixtures also exhibited a volume reduction with increasing kaolin content.

Figure 5 presents the initial, post-saturation and post-consolidation void ratio of the samples. The left section of the graph shows the initial void ratios of the mixtures tested both in the standard apparatus and in *FROZEN*. The central section reports the void ratios after saturation, while the right section presents the final values measured after consolidation under the designated effective confining pressure for each test. Two key observations can be made:

- The initial void ratio does not always consistently align with the theoretical value ($e_{theor} = 0.74$), due to variability during sample preparation.
- Soil compaction during saturation and consolidation increases with higher kaolin content.

The trend observed during the consolidation phase is consistent across both the standard triaxial apparatus and the *FROZEN* device. While absolute void ratio values may differ between specimens – primarily due to slight variations in the initial conditions and entity of saturation collapse (Fig. 4*b*) – the reduction in void ratio with increasing effective confining pressure follows a similar trend in both setups when comparing tests conducted at the same target pressure.

At the microscale level, a possible transition from bimodal to monomodal PSD is expected when collapse for saturation occurs. This transition is attributed to a decrease in macroporosity, accompanied by a slight increase in microporosity. This increase occurs as the aggregates expand with rising water content; however, the effect remains minimal due to kaolin's low reactivity as a non-active clay (Della Vecchia et al. 2015). The consolidation phase further influences macroporosity, resulting in additional compaction (Alonso et al. 2013).

3.2. Freezing phase

During the freezing phase, as the thermal load progresses, the freezing front (i.e., the boundary between frozen and unfrozen soil) propagates through the sample. The residual liquid water may either be drawn toward the freezing front or expelled from the sample, depending on the interplay of attractive forces at the freezing front, repulsive forces from ice expansion, and the soil permeability.

To monitor the progression of the freezing front, temperature measurements are collected and interpolated using the kriging method, a statistical approach that utilizes a linear combination of data points. Specifically, thermocouples positioned within the sample (designated as A, B, C, D, E, F, G, H, and I in Fig. 2*b*) provide boundary conditions (BCs) for the external edges. The temperature readings from the thermocouples within the inner copper tube (designated as "in" and "out" in Fig. 2*b*) are used as BCs for the inner vertical face of the sample, leveraging the high thermal conductivity of the copper tube to maintain accuracy.

The interpolation procedure applied to all tests is described here for the sample S85K15-50, as an example. Figure 6 presents the temperature contours, with only half of the sample width depicted for symmetry. The horizontal axis begins 5 mm away from the sample symmetry axis, aligning with the inner surface of the sample that is in contact with the 10 mm thick copper tube.

The freezing front is represented by the 0 °C isotherm, indicated through a yellow line. After 3 h of freezing, only the upper right corner of the sample is still unfrozen, while by 6 h, the entire sample has frozen.

Each soil mixture displays distinct behavior in terms of hydro-mechanical response during the freezing process, particularly regarding water migration and volumetric strain. Figure 7 illustrates the behavior of the three investigated mixtures under varying confining pressures. For pure sand, the freezing process remains largely unaffected by confinement and proceeds at constant void ratio. In fact, the phase change of liquid water to solid ice gives rises to a local expansion and a fast drainage of the liquid water displaced by ice due to the high permeability of the unfrozen sand. This leads to a measurable outflow of water from the sample, comparable to 9% of the volume of liquid water available in the sample, with no significant overall volumetric strain observed.

Fig. 6. Isothermal curves during the freezing process for S85K15-50: half of the sample is represented for symmetry, at four time steps.

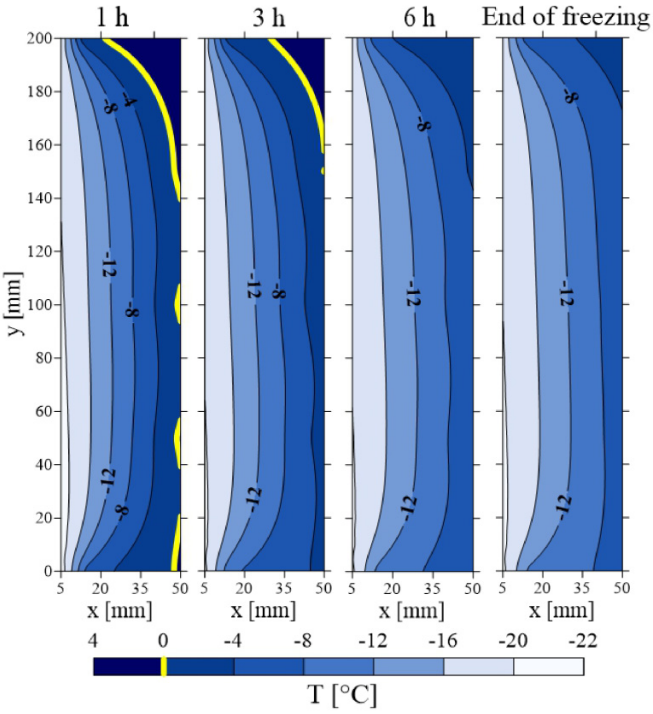

When 7.5% kaolin is added to the sand, the behavior changes slightly. Although no deformation is observed during freezing, the hydraulic response is affected by confining pressure. At lower confinement, cryogenic suction induces water inflow toward the freezing front, whereas at higher confinement levels, the repulsive forces generated by ice formation at the freezing front result in water outflow.

For the mixture containing 15% kaolin, a more pronounced dependency on confining pressure is observed. At a confinement level of 50 kPa, significant swelling occurs, driven by cryogenic suction, which encourages water inflow toward the freezing front, in conjunction with reduced permeability of the soil. As the confining pressure increases, the swelling is progressively restrained, and at the highest confinement level, no volumetric strain is detected. Under these conditions, the forces exerted by ice formation dominate, leading to water outflow.

The phenomenon of frost heave is mainly driven by the amount of water that can migrate to the freezing front, drawn by cryogenic suction. Finer particles play a crucial role in surface tension effects and suction, which lower the

Fig. 7. Water ratio variation (Δe_w) and void ratio variation (Δe) of the mixtures during freezing, with increasing confining pressure.

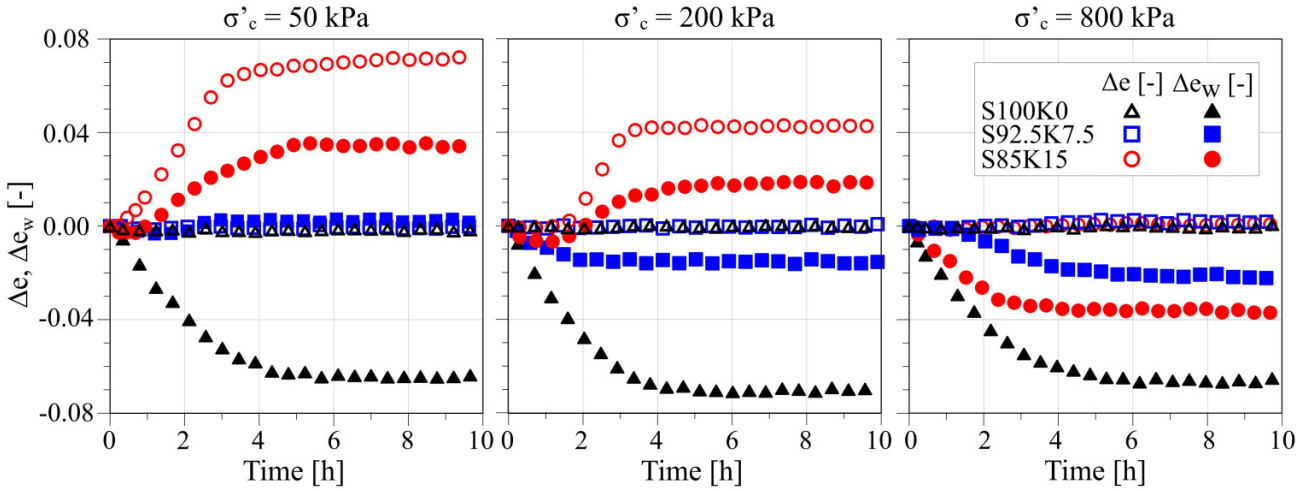

freezing point of the water surrounding the particles and smooth the transition interval between the unfrozen and frozen state (Vu et al. 2022). This mechanism facilitates water migration along preferential pathways. While kaolin is typically classified as a non-active clay with lower suction potential, its presence within a coarse matrix still facilitates cryogenic suction-driven water movement. With increasing activity of the fine particles, frost heave may be exacerbated. Generally, the threshold fine content required to induce frost heave depends on multiple factors, including particle size distribution, grading, and mineralogy (Carter and Bentley 2016). In this study, frost heave is only observed in the mixture containing 15% kaolin. It results to be highly frost-susceptible, with frost-heaving ratios of 4.4% at a confinement of 50 kPa and 2.7% at 200 kPa.

It is worth noting that a threshold of 1% radial deformation was adopted as a preliminary benchmark to assess frost susceptibility within the *FROZEN* apparatus. This criterion is supported by the observation that axial deformations measured during the tests were consistently less than 10% of the radial ones, and therefore the radial component largely dominates the deformation process under the adopted setup. However, when full 3D frost heave occurs, multidimensional effects must be taken into account (Yang et al. 2024).

The tests S92.5K7.5-50, S85K15-50, and S85K15-200 exhibited a net water intake during the freezing process. However, an initial outflow of water was observed, consistent with findings in the literature (Zhou et al. 2014), which indicate that the initial formation of ice displaces unfrozen water before cryogenic suction becomes the dominant mechanism driving water movement.

The rate of thermal load progression during freezing is assessed at the mid-height of the samples, using the temperature data recorded 100 mm from the base of the specimen at the external surface (thermocouple E in Fig. 2*b*). As an example, Fig. 8 shows the trend in temperature and freezing speed over time for samples S100K0-50, S92.5K7.5-50, and S85K15-50. The freezing speed consistently reaches its peak within the temperature range of 0 to −2 °C, corresponding to the phase transition of supercooled water into ice, accompanied by energy release. In pure sand, the peak freezing speed is slightly higher than in the mixtures, likely due to the greater volume of water undergoing the phase change (Vu et al. 2022). This energy release facilitates a faster propagation of the thermal front in pure sand. Furthermore, the formation of ice significantly increases the thermal conductivity of the three-phase system (liquid water, ice, and soil). In contrast, the presence of kaolin reduces the ice content within the pores, resulting in lower thermal conductivity in frozen sand–clay mixtures compared to frozen pure sand (Vu 2022).

It is worth noting that during the freezing process, water movement within the drainage system ceases only once the entire sample has reached subzero temperatures. A comparison between the temperature distribution (Fig. 6) and the hydro-mechanical behavior (Fig. 7) for sample S85K15-50 shows that, after 3 h of freezing, most of the sample has reached negative temperatures, except for a small unfrozen region in the upper corner. At this point, the drainage system remains unfrozen, as water inflow continues until approximately 6 h into the freezing process. This indicates that the sample remains capable of draining during freezing, and by the time the drainage system freezes, the sample is already fully frozen. Notably, this behavior was consistently observed across all tests.

4. Results' interpretation and implications

The behavior of the three mixtures under freezing conditions necessitates an in-depth analysis to interpret the observed phenomena and identify factors that require further investigation. A crucial aspect to examine is the evolution of ice and liquid water saturation within the pores, and so the temporal development of the three-phase soil–water–ice system. The following subsections explore the thermo-hydraulic

Fig. 8. Temperature and freezing speed trends over time for three specimens.

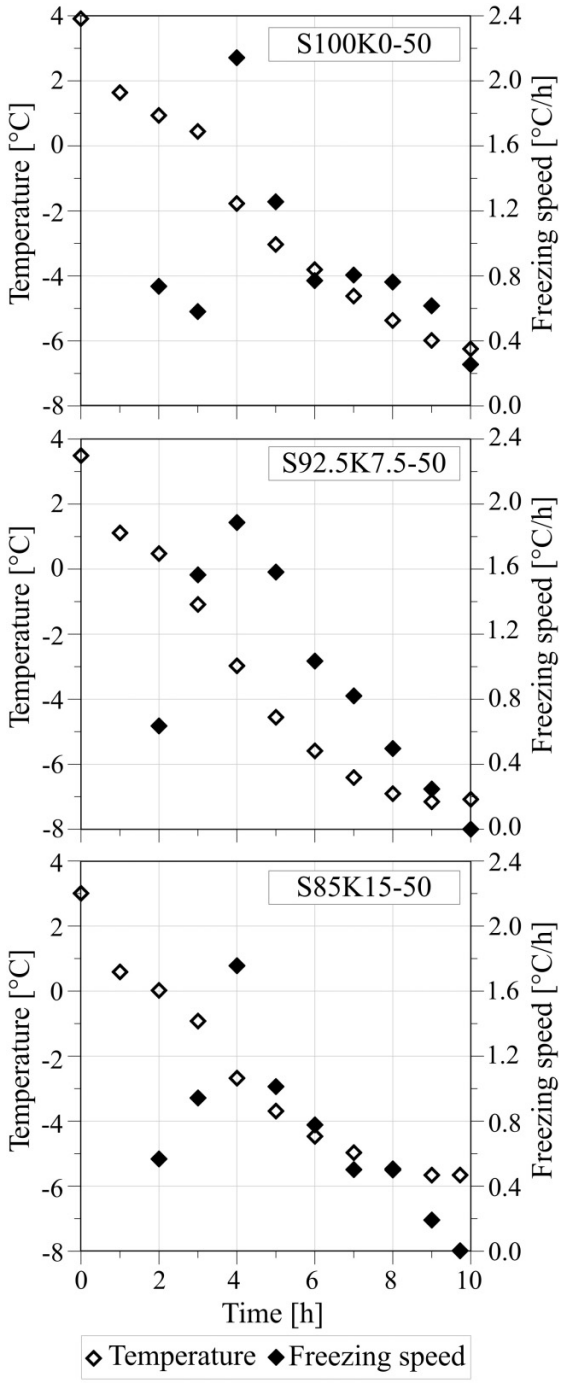

behavior of the mixtures, focusing on the changes in liquid water saturation degree and effective permeability, as well as the mechanical response to freezing.

4.1. Liquid water saturation degree

The objective at the end of the freezing phase is to achieve a steady-state condition throughout the sample, with a temperature distribution that enables the liquid water saturation level to reach its residual value uniformly. The SFRC is essential to effectively interpret the experimental results. It estimates the distribution of liquid saturation in soils as a function of temperature and is typically derived by combining the thermodynamic equilibrium equation with a freezing characteristic function. The thermodynamic equilibrium between liquid water and ice is given by the integrated form of the Clausius–Clapeyron equation:

$$P_i = \frac{\rho_i}{\rho_l} P_l - \rho_i l \ln\left(\frac{T}{273.15}\right) \quad (4)$$

where P represents the pressure, ρ is mass density, l is the specific latent heat of fusion, and T is temperature. The subscripts i and l denote ice and liquid water, respectively.

The freezing characteristic function correlates the unfrozen water saturation with the thermodynamic properties of the soil. Numerous formulations have been proposed in the literature. As highlighted by Wang et al. (2025), these can be broadly classified into four main categories: (i) empirical equations derived from fitting experimental data; (ii) equations based on intrinsic soil properties; (iii) models adapted from unsaturated soil mechanics, in analogy with soil water retention curves; and (iv) physically based models that incorporate parameters such as the PSD. In this study, a widely adopted freezing characteristic function originally proposed by Van Genuchten (1980) for unsaturated soils – and subsequently adapted to account for the behavior of freezing soils – is used to interpret the experimental results. It is expressed as

$$S_e = \frac{S_l - S_{res}}{1 - S_{res}} = \left[1 + \left(\frac{P_i - P_l}{P_0}\right)^{\frac{1}{1-m}}\right]^{-m} \quad (5)$$

where S_e is the effective degree of saturation, S_l is the liquid water saturation, so that $S_l + S_i = 1$ with S_i the ice saturation, S_{res} is the residual degree of saturation, P_0 is the ice-entry value, and m is a material constant. In eq. 5, a saturated initial condition is assumed. By combining the two equations, the following relation is obtained (Nishimura et al. 2009):

$$S_e = \left\{1 + \left[\frac{-\left(1 - \frac{\rho_i}{\rho_l}\right) P_l - \rho_i l \ln\left(T/273.15\right)}{P_0}\right]^{\frac{1}{1-m}}\right\}^{-m} \quad (6)$$

For the purposes of this study, P_l is neglected. eq. 6 is calibrated using experimental values of SFRCs reported by Vu et al. (2022) for both pure sand and a sand–kaolin mixture containing 15% kaolin. No SFRC was available from literature for the mixture containing 7.5% kaolin; therefore, it was predicted through interpolation of available literature experimental data on the other two mixtures. Figure 9 reports the SFRCs of the three materials.

The main differences between pure sand and the mixtures are twofold: (1) the temperature of spontaneous nucleation shifts to lower values with increasing kaolin content and (2) the residual liquid saturation degree rises with kaolin content. In contrast, the slope of the SFRC is not significantly influenced by the presence of fines in the sandy matrix. This is reflected in similar values of m in eq. 6, as shown in Table 4,

Fig. 9. Soil freezing retention curves (SFRCs) for the tested sand–clay mixtures. The label *Ref* refers to results from Vu et al. (2022), *and FROZEN* refers to the tests conducted in this study. "Exp" denotes the experimental data points, and "VG" denotes the fitted Van Genuchten model.

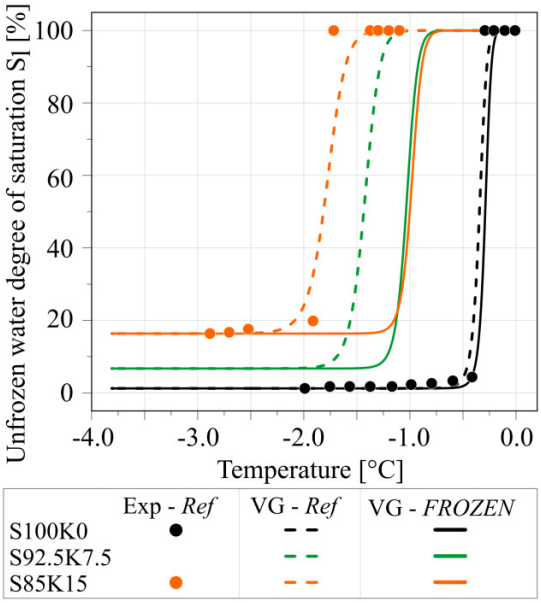

which summarizes the calibrated Van Genuchten parameters for pure sand and the sand–kaolin mixtures.

The SFRCs presented in this study have been adjusted to reflect the varying initial void ratio of the samples under investigation (the void ratio e in Table 4, with respect to the void ratio e_0 of the literature work). In this regard, the authors refer to the literature on unsaturated soils, relying on the analogy with frozen soils. According to Gallipoli (2012), changes in void ratio primarily affect larger pores, while smaller pores remain unchanged. This suggests that at high suction levels, induced by microporosity, the soaking curves corresponding to different void ratios converge into a single relationship between water ratio and suction. Thus, applying the Van Genuchten (1980) model, it is expected a modification in the air-entry value (and similarly in the ice-entry value) while maintaining a nearly constant residual degree of saturation.

Gallipoli et al. (2003) also proposed an extension of the Van Genuchten model to account for the effects of changing void ratio e. The air-entry value P_0 in eq. 5 varies with e according to the following expression:

$$P_0 = \frac{\omega}{e^{\Psi}} \tag{7}$$

where ω and Ψ are soil-specific parameters. To the authors' knowledge, existing literature has not thoroughly explored the influence of varying void ratio on the SFRC for the mixtures considered in this work. Therefore, for simplification, a unitary value of Ψ is assumed, which facilitates the calculation of ω. The resulting trend of P_0 against e was critically analyzed and compared with trends from other established models (e.g., Mašín 2010) to validate the assumption of $\Psi = 1$.

The values of P_0 for the prefreezing void ratio conditions of the tests conducted are summarized in Table 4. At this point, Fig. 9 illustrates the SFRCs derived from the Van Genuchten model, fitting the experimental results obtained by Vu et al. (2022) and showing shifted trends for the conditions of the samples in this work (*FROZEN*), taking into account the different void ratios. The graph represents the unfrozen water saturation degree $S_l = S_e(1 - S_{res}) + S_{res}$. The residual saturation degrees (S_{res}) for S100K0 and S85K15 are reported in the literature (Vu et al. 2022) as 0.012 and 0.163, respectively. For the intermediate mixture, S92.5K7.5, the residual saturation degree is determined through interpolation, yielding a value of 0.067.

As observable in Fig. 9, the gap between the SFRCs derived from the literature and those obtained for the tests of this study increases with higher kaolin content. However, the interpolation used to estimate the SFRC for the S92.5K7.5 mixture produced a trend that remains below that observed for the S85K15 mixture. This deviation from the expected progression may highlight limitations in the interpolation method and the application of partially saturated soil mechanics for defining freezing parameters—especially in the absence of direct experimental data, as is the case for the 7.5% kaolin mixture. Furthermore, as shown in Table 4, the m value used for the S85K15 mixture was also applied to the S92.5K7.5 mixture, which may have contributed to the observed discrepancy in the trends.

As an example, Fig. 10 illustrates the interpolation of the liquid water saturation degree during the freezing process, with the freezing front marked in yellow, for the test S85K15-50, whose temperature distribution is depicted in Fig. 6. Two main observations can be made:

- At the end of the freezing process, the entire sample achieves a residual liquid saturation value.
- The transition zone between saturated conditions ($S_l = 1$) and residual conditions (represented by the color gradient from blue to nearly white) is relatively narrow. This is attributed to the steep slope of the SFRCs, which restricts the temperature range over which the transition occurs.

These observations have been consistently validated across all freezing tests conducted.

Although the Van Genuchten model employed in this study does not explicitly incorporate confining pressure as a parameter, literature indicates that mechanical stress can influence the freezing behavior of soils. In particular, increased confining pressure has been shown to slightly reduce the temperature of initial ice nucleation and significantly raise the residual unfrozen water content, especially in fine-grained soils due to their higher capillarity and adsorptive capacity (Mu et al. 2019; Wang et al. 2025). The distribution presented in Fig. 10 refers to the sample tested under the lowest confining pressure. Therefore, in this case we expect that the influence of confinement on the estimated liquid saturation profile is limited. However, we recognize that at higher confining pressures, the impact on freezing dynamics and water

Table 4. Parameters of the Van Genuchten soil freezing retention curves (SFRCs) for the mixtures.

		Vu et al.			This study		
Material	m	e_0 (−)	P_{0,e_0} (kPa)	k_{sat,e_0} (m/s)	e (−)	$P_{0,e}$ (kPa)	$k_{sat,e}$ (m/s)
S100K0	0.9	0.59	380	1.00×10^{-4}	0.7	320	1.64×10^{-4}
S92.5K7.5	0.95	–	1600	6.00×10^{-6}	0.61	1154	1.6×10^{-5}
S85K15	0.95	0.33	2000	8.50×10^{-8}	0.6	1100	5.11×10^{-7}

Fig. 10. Liquid water saturation degree distribution based on the estimated SFRC for sample S85K15-50.

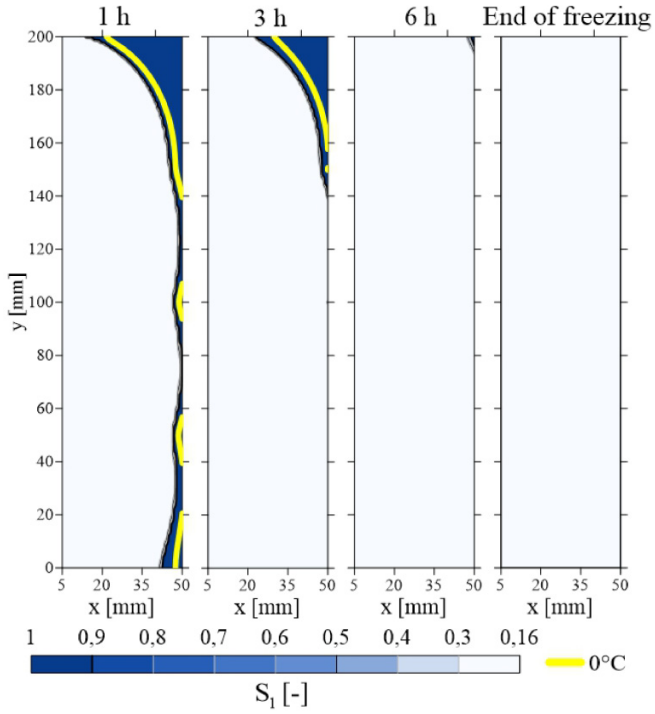

redistribution could be more pronounced, potentially leading to different saturation trends.

For this reason, future developments should focus on adopting or developing more advanced SFRC models that explicitly incorporate the role of confining pressure, to more accurately capture the coupled hydro-mechanical behavior of freezing soils under varying stress conditions.

4.2. Soil effective permeability evolution

The effective permeability k_{eff} is derived from the SFRC, following a common approach established in the literature (Casini et al. 2023). Specifically, the relative hydraulic conductivity (k_{rel}) is multiplied by the intrinsic permeability (k_{sat}). The relative hydraulic conductivity, as defined by Van Genuchten (1980), is expressed as follows:

$$k_{rel} = \frac{k_{eff}}{k_{sat}} = \sqrt{S_e}\left(1 - \left(1 - S_e^{1/m}\right)^m\right)^2 \quad (8)$$

where m is a material parameter corresponding to the one used to define the effective degree of saturation in eq. 6 (Nishimura et al. 2009). The value of k_{sat} is obtained from Vu (2022), adjusted for variations in prefreezing void ratio using an equation proposed by Ren and Santamarina (2018). These latter authors observed a relationship between hydraulic conductivity (k) and void ratio (e) across a wide range of materials, resulting in the following equation:

$$k = k_0\left(\frac{e}{e_0}\right)^{\beta} \quad (9)$$

with k_0 being the permeability of the material with void ratio e_0 and β a sensitivity parameter. This last is known to vary depending on soil type and texture. Based on an extensive dataset of 123 soils, Ren and Santamarina (2018) reported that β typically ranges between 2 and 6, with coarse-grained soils (such as sands and silts) generally falling within the range of 2–4. Higher values are associated with more plastic, fine-grained soils. Given the gap-graded nature of the tested sand–kaolin mixtures—characterized by a coarse-grained matrix with a limited addition of low-activity fines—it is reasonable to assume an average value of $\beta = 3$. A sensitivity analysis was carried out by varying β between 2 and 4, showing only limited variation of k across this range.

In this study, eq. 9 is applied to estimate k_{sat} prior to freezing. The values used and results obtained are summarized in Table 4, revealing that k_{sat} is significantly higher in the here tested samples than in the reference literature samples with void ratio e_0. Consequently, the estimated trends of soil effective permeability as a function of temperature are presented (Fig. 11). Since no experimental data are available in the literature for the S92.5K7.5 mixture, and the SFRC derived through interpolation (Fig. 9) – based on trends from the other two materials – shows limitations due to the lack of direct validation, the hydraulic permeability trend is presented only for pure sand and the sand with 15% kaolin.

Several important aspects emerge from the permeability trends of S100K0 and S85K15. Firstly, the unfrozen permeability of pure sand is significantly greater than that of the sand–kaolin mixture, facilitating water to flow out of the sand. Additionally, the temperature at which water begins to freeze is lower in the sand–clay mixture.

A further notable observation is the difference in the transition interval between unfrozen and residual permeability. In pure sand, the high permeability allows for rapid water flow, but the system quickly shifts from unfrozen to residual permeability, leading to almost instantaneous local freezing. Conversely, the S85K15 mixture exhibits a more gradual transition, as reflected in the gentler slope of its curve compared to the steeper slope of the S100K0 curve in Fig. 11. This behavior suggests that, under the same freezing speed, ice

Fig. 11. Soil effective permeability trends for the tested samples calculated according to the Van Genuchten model. The line in black is the S100K0 mixture, while the one in orange is the S85K15 mixture.

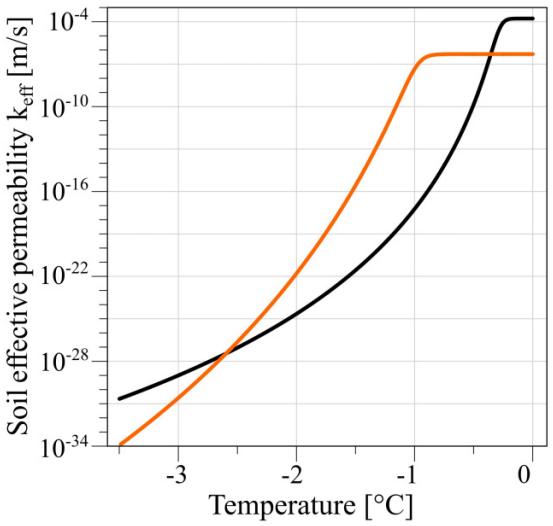

formation in the pores of the S85K15 mixture occurs more slowly, extending the transition over a broader temperature range. This prolonged interval allows microcryogenic forces to develop, unlike in pure sand, where the rapid permeability drop limits cryogenic ice–water interactions. As illustrated in Fig. 7 and previously discussed, for samples S85K15-50 and S85K15-200, this process results in water inflow into the sample and leads to sample swelling. However, at higher confinement levels, where expansion is restricted, this behavior is no longer observed.

4.3. Soil deformation upon freezing

When considering soil deformation during freezing, it is generally expected that the expansion of water within the pores leads to a volumetric increase of approximately 9%. However, the SFRCs indicate that a portion of the water remains unfrozen, referred to as the residual unfrozen water content. Since the systems here analyzed are saturated, this residual water content is expressed as the void ratio filled by unfrozen water, e_{uw}, calculated by multiplying the residual liquid water saturation degree S_{res} by the prefreezing void ratio $e_{prefreezing}$. The volume of voids contributing to water expansion during freezing, referred to as Δe_{active}, is defined as follows:

$$\Delta e_{active} = e_{prefreezing} - e_{uw} \quad (10)$$

Then, the expected theoretical expansion $\Delta e_{i,th}$ is calculated as

$$\Delta e_{i,th} = 0.09 \Delta e_{active} \quad (11)$$

For a complete discussion of the obtained results, $\Delta e_{i,th}$ is compared to Δe_{ice}, which is calculated as the difference between the measured quantities Δe and Δe_w (eq. 1). The comparison is illustrated in Fig. 12, where, referring to the pure sand results, the theoretical expansion $\Delta e_{i,th}$ aligns with the measured Δe_{ice}. This confirms the physical process occurring within the samples: as the freezing front advances, water expands by 9%, theoretically causing a swelling of $\Delta e_{i,th}$. However, due to the open drainage conditions, the remaining liquid water is expelled from the sample. The high permeability allows complete drainage of the unfrozen water, compensating for the ice-induced expansion, and thus no significant deformation is observed.

Fig. 12. Comparison between theoretical ($\Delta e_{i,th}$) and experimental ice expansion (Δe_{ice}) at the end of the freezing process.

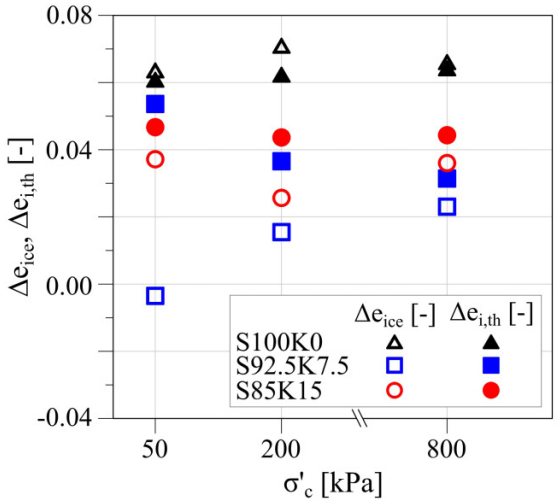

In the mixture containing 15% kaolin, a close match between the theoretical and experimental changes in void ratio due to water turning into ice, even when water inflow and swelling occur due to cryogenic suction (as observed in the tests at 50 and 200 kPa of confinement in Fig. 7), is appreciable.

The behavior of the intermediate mixture (7.5% kaolin) requires further investigation. In this case, there is a discrepancy between the theoretical ($\Delta e_{i,th}$) and the experimental expansion (Δe_{ice}). Additionally, the amount of water expelled from the sample is insufficient to fully compensate for the expansion caused by freezing. No swelling is observed, and as the confining pressure increases, cryogenic suction is suppressed, leading to water outflow. While the difference between $\Delta e_{i,th}$ and Δe_{ice} decreases under higher confinement, it still remains unresolved. A microscale analysis may be necessary to better understand how the interaction between sand and kaolin particles influences key factors such as cryogenic suction, water–ice expansion, and the presence of unfrozen water that does not participate in the freezing process.

4.4. Insights from related works

The experimental results presented in this study are consistent with findings reported in the literature regarding the influence of fine content and confining pressure on frost-induced deformation and water migration. Several previous studies have highlighted how the presence of fine

particles affects unfrozen water content and the development of cryogenic suction. The interpretation of our results is strongly supported by the study of Vu et al. (2022), which serves as a key reference for understanding the freezing behavior of sand–clay mixtures. Beyond Vu et al. (2022), several researchers have explored the effect of fines on frost heave. Konrad (2005) reported a progressive increase in frost-induced strains with increasing fine content in natural aggregate mixtures, underscoring the contribution of fines to heave potential. Similarly, Li et al. (2017) and Gao et al. (2018) observed a nearly linear increase in frost heave with fine content, often identifying a threshold below which frost effects were minimal. Notably, Long et al. (2018) found that only mixtures containing more than 15% kaolin showed measurable frost-induced strains – a finding that aligns closely with the present study. Nevertheless, many of these studies utilized natural or site-specific soils with heterogeneous compositions, limiting the generalizability of their conclusions. In contrast, the present study employed controlled laboratory mixtures, offering more consistent and interpretable results.

Furthermore, prior works were predominantly conducted under 1D freezing conditions. This represents a key limitation when compared to our approach. The triaxial setup used in this research permits:

- application of confining pressure and axial stress indipendently;
- axis-symmetric specimen deformation;
- bidirectional drainage from both horizontal faces.

These features allow a more realistic representation of field conditions encountered in AGF applications, where multidirectional stress states and complex water migration paths occur. The findings of this work are further supported by the results of Bartoli et al. (2020), who carried out preliminary tests using the same FROZEN apparatus on a well-graded natural silty soil, composed of approximately 45% sand, 42% silt, and 12% clay. Although the study was based on a site-specific material – thus not directly comparable to standardized mixtures – the experimental conditions were similar, particularly in terms of applied confining stress and drainage setup. The results confirmed trends observed in the current study: under freezing, void ratio increased along with water inflow, while an initial phase of water outflow was detected prior to ice formation. These findings reinforce the proposed interpretation of the interplay between fine content and water migration under freezing conditions.

5. Conclusions

This study improves the understanding of AGF in intermediate soils by systematically analyzing the impact of fine content and confining pressure on frost susceptibility and water migration. This wide experimental campaign provides an insight into the role of fine content and confining stress prior to freezing in a sandy matrix. The use of a modified triaxial apparatus replicating in situ conditions ensures the relevance of the findings to real-world AGF applications.

Kaolin was added to the sand in proportions of 0%, 7.5%, and 15%, and the thermo-hydro-mechanical behavior of the resulting mixtures during freezing was examined at three consolidation pressures (50, 200, and 800 kPa), selected to represent typical stress conditions at different depths in AGF applications (from shallower to deeper). Continuous monitoring of the displacements (radial and axial) and the water movement in the drainage system during freezing allow to distinguish the thresholds at which fine content begins to affect frost susceptibility, and to observe transitional behaviors.

A key contribution of this work is the identification of complex interactions between cryogenic suction and confining pressure, particularly in gap-graded soils with moderate fine content. The results show that while pure sand and the 7.5% kaolin mixture are non-frost-susceptible, the latter is characterized by water inflow without measurable expansion, indicating a complex balance between ice formation and water retention within the pore structure. This highlights the need for further microscale investigations into ice–liquid interactions.

Moreover, the study demonstrates that the presence of 15% kaolin significantly alters the freezing behavior, making the mixture highly frost-susceptible under low confinement but completely suppressing expansion at high confining pressures. These insights refine existing AGF design considerations by providing quantitative evidence of how soil composition and stress conditions influence deformation and water transport during freezing.

From a practical standpoint, these findings contribute to the understanding of the role of the different confining stress (or in situ depth) and fine content on the AGF-induced heave. Looking ahead, while the 1% frost heave threshold adopted in this study provides a useful first approximation for identifying frost-susceptible soils under radial freezing conditions, its general applicability must be critically assessed. Future investigations should aim to experimentally compare 1D and 3D frost heave scenarios, in order to refine existing criteria and develop more robust thresholds. These studies will be essential for improving the characterization of frost effects in real-world applications, where deformation may not be constrained to a single direction.

Additionally, although the present study provides a macroscale perspective and offers qualitative and semiquantitative insights into moisture migration during freezing, future research could aim to investigate the microstructural evolution of freezing mixtures. Advanced monitoring techniques – such as time-resolved imaging, high-resolution moisture sensors, or microscale observation methods – could be employed to capture the dynamic redistribution of water within the soil matrix. Such approaches would enhance the understanding of the coupled thermo-hydro-mechanical mechanisms that govern the frost response of intermediate soils.

Then, exploring the applicability and potential limitations of models from unsaturated soil mechanics to explain the behavior of freezing soils – such as the Van Genuchten framework – could further enhance its description in coarse–fine mixtures. Such models may require adaptation or parameter

optimization to effectively capture the coupled processes observed in experimental settings.

Finally, while it is well established that frozen soils generally exhibit increased strength relative to their unfrozen state, the mechanical behavior of intermediate soils in their frozen state remains largely site specific. Ongoing experimental studies aimed at producing general findings will be essential to advancing and standardizing knowledge of the thermo-hydro-mechanical behavior of soils subjected to AGF.

Acknowledgements

The second author acknowledges financial support from LazioInnova for funding the FROZEN project (FILAS-RU-2014-1180). Technical support and valuable discussions from Andrea Viglianti and Manuel Bartoli during the experimental campaign are also acknowledged.

Article information

History dates

Received: 24 December 2024
Accepted: 19 September 2025
Accepted manuscript online: 26 September 2025
Version of record online: 12 November 2025

Copyright

Data availability

Data generated or analyzed during this study are available from the corresponding author upon reasonable request.

Author information

Author ORCIDs

Giulia La Porta https://orcid.org/0000-0001-5727-4289
Francesca Casini https://orcid.org/0000-0001-7933-9055
Marina Pirulli https://orcid.org/0000-0001-8400-1569

Author contributions

Conceptualization: GLP, FC
Data curation: GLP
Formal analysis: GLP
Funding acquisition: MP
Investigation: GLP
Methodology: GLP, FC
Project administration: MP
Supervision: FC, MP
Validation: GLP
Visualization: GLP
Writing – original draft: GLP
Writing – review & editing: GLP, FC, MP

Competing interests

The authors declare that there are no competing interests.

References

Alonso, E.E., Pinyol, N., and Gens, A. 2013. Compacted soil behaviour: initial state, structure and constitutive modelling. Géotechnique, **63**(6): 463–478.

Al-Tabbaa, A., and Wood, D.M. 1987. Some measurements of the permeability of kaolin. Geotechnique, **37**(4): 499–514. doi:10.1680/geot.1987.37.4.499.

Andersland, O.B., and Ladanyi, B. 2003. Frozen ground engineering. John Wiley & Sons, Hoboken, New Jersey, USA.

Arenson, L.U., and Springman, S.M. 2005. Mathematical descriptions for the behaviour of ice-rich frozen soils at temperatures close to 0 °C. Canadian Geotechnical Journal, **42**(2): 431–442. doi:10.1139/t04-109.

Arenson, L.U., Johansen, M.M., and Springman, S.M. 2004. Effects of volumetric ice content and strain rate on shear strength under triaxial conditions for frozen soil samples. Permafrost and Periglacial Processes, **15**(3): 261–271. doi:10.1002/ppp.498.

ASTM. 2020. ASTM D7181-20. Standard test method for consolidated drained triaxial compression test for soils. ASTM, USA.

Bartoli, M., Casini, F., and Grossi, Y. 2020. Geotechnical characterization of an artificially frozen soil with an advanced triaxial apparatus. *In* Tunnels and underground cities: Engineering and innovation meet archaeology, architecture and art. CRC Press, London, UK. pp. 646–654.

Boussaid, K. 2005. Sols intermédiaires pour la modélisation physique. Ph.D. thesis, École Centrale de Nantes et Université de Nantes, Nantes, France.

Cai, C., Ma, W., Zhou, Z., Mu, Y., Zhao, S., Chen, D., and Liao, M. 2019. Laboratory investigation on strengthening behavior of frozen China standard sand. Acta Geotechnica, **14**(1): 179–192. doi:10.1007/s11440-018-0648-3.

Carter, M., and Bentley, S.P. 2016. Soil properties and their correlations. 2nd ed. John Wiley & Sons, Hoboken, New Jersey, USA, New Jersey, USA. doi:10.1002/9781119130888.

Casini, F., Vaunat, J., and Romero, E. 2012. Consequences on water retention properties of double-porosity features in a compacted silt. Acta Geotechnica, (7): 139–150. doi:10.1007/s11440-012-0159-6.

Casini, F., Guida, G., Restaini, A., and Celot, A. 2023. Water retention curve–based design method for the artificial ground freezing: the Isarco River Underpass tunnels within the Brenner Base Tunnel Project. Journal of Geotechnical and Geoenvironmental Engineering, **149**(3): 1–15. doi:10.1061/JGGEFK.GTENG-10723.

Chen, H., Guo, H., Yuan, X., Chen, Y., and Sun, C. 2020. Effect of temperature on the strength characteristics of unsaturated silty clay in seasonal frozen region. KSCE Journal of Civil Engineering, **24**(9): 2610–2620. doi:10.1007/s12205-020-1974-1.

Della Vecchia, G., Dieudonné, A.c., Jommi, C., and Charlier, R. 2015. Accounting for evolving pore size distribution in water retention models for compacted clays. International Journal for Numerical Methods in Geomechanics, **39**(2014): 702–723. doi:10.1002/nag.

El Dine, B.S., Dupla, J.C., Frank, R., Canou, J., and Kazan, Y. 2010. Mechanical characterization of matrix coarse-grained soils with a large-sized triaxial device. Canadian Geotechnical Journal, **47**(4): 425–438. doi:10.1139/T09-113.

Esmaeili-Falak, M., Katebi, H., and Javadi, A. 2018. Experimental study of the mechanical behavior of frozen soils—a case study of Tabriz Subway. Periodica Polytechnica–Chemical Engineering, **62**(1): 117–125. doi:10.3311/PPci.10960.

Ferrigno, A. 2019. Comportamento termo-idro-meccanico dei terreni artificialmente congelati: studio sperimentale e numerico. Master's thesis, Università degli Studi di Roma Tor Vergata, Rome, Italy.

Gallipoli, D. 2012. A hysteretic soil-water retention model accounting for cyclic variations of suction and void ratio. Geotechnique, **62**(7): 605–616. doi:10.1680/geot.11.P.007.

Gallipoli, D., Wheeler, S.J., and Karstunen, M. 2003. Modelling the variation of degree of saturation in a deformable unsaturated soil. Geotechnique, **53**(1): 105–112. doi:10.1680/geot.2003.53.1.105.

Gao, J., Lai, Y., Zhang, M., and Feng, Z. 2018. Experimental study on the water-heat-vapor behavior in a freezing coarse-grained soil. Applied Thermal Engineering, **128**: 956–965. doi:10.1016/j.applthermaleng.2017.09.080.

Gens, A. 2010. Soil-environment interactions in geotechnical engineering. Geotechnique, **60**(1): 3–74. doi:10.1680/geot.9.P.109.

Guida, G., Pucci, A., Romani, E., Viggiani, G.M., and Casini, F. 2025. Interpretation of an artificial ground freezing field trial at fori imperiali in rome. Underground Space, **23**: 89–112.

Haβ, H., and Schäfers, P. 2005. Application of ground freezing for underground construction in soft ground. *In* Proceedings of the 5th International Symposium TC28. Amsterdam, Netherlands. pp. 405–412. Taylor & Francis, London, UK. doi:10.1007/978-3-319-73568-9_174.

Hu, J., Liu, Y., Li, Y., and Yao, K. 2018. Artificial ground freezing in tunnelling through aquifer soil layers: a case study in Nanjing Metro Line 2. KSCE Journal of Civil Engineering, **22**(10): 4136–4142. doi:10.1007/s12205-018-0049-z.

Kenney, T., Van Veen, W., Swallow, M., and Sungaila, M. 1992. Hydraulic conductivity of compacted bentonite-sand mixtures. Canadian Geotechnical Journal, **29**(3): 364–374.

Konrad, J.M. 2005. Estimation of the segregation potential of fine-grained soils using the frost heave response of two reference soils. Canadian Geotechnical Journal, **42**(1): 38–50. doi:10.1139/t04-080.

Konrad, J.M. 2008. Freezing-induced water migration in compacted base-course materials. Canadian Geotechnical Journal, **45**(7): 895–909. doi:10.1139/T08-024.

Lade, P.V., Liggio, C.D., and Yamamuro, J.A. 1998. Effects of non-plastic fines on minimum and maximum void ratios of sand. Geotechnical Testing Journal, **21**(4): 336–347. doi:10.1520/gtj11373j.

Lai, Y., Xu, X., Yu, W., and Qi, J. 2014. An experimental investigation of the mechanical behavior and a hyperplastic constitutive model of frozen loess. International Journal of Engineering Science, **84**: 29–53. doi:10.1016/j.ijengsci.2014.06.011.

Li, A., Niu, F., Zheng, H., Akagawa, S., Lin, Z., and Luo, J. 2017. Experimental measurement and numerical simulation of frost heave in saturated coarse-grained soil. Cold Regions Science and Technology, **137**: 68–74. doi:10.1016/j.coldregions.2017.02.008.

Long, X., Cen, G., Cai, L., and Chen, Y. 2018. Experimental research on frost heave characteristics of gravel soil and multifactor regression prediction. Advances in Materials Science and Engineering, **2018** (37): 1–13. doi:10.1155/2018/5682619.

Lo Presti, D., Pallara, O., Raino, M., and Maniscalco, R. 1994. A computer-controlled triaxial apparatus: Preliminary results. Rivista Italiana di Geotecnica, **28**(1) 43–60.

Mašín, D. 2010. Predicting the dependency of a degree of saturation on void ratio and suction using effective stress principle for unsaturated soils. International Journal for Numerical Methods in Geomechanics, **34**: 73–90. doi:10.1002/nag.

Mu, Q., Zhou, C., Ng, C.W.W., and Zhou, G. 2019. Stress effects on soil freezing characteristic curve: equipment development and experimental results. Vadose Zone Journal, **18**(1): 1–10.

Nishimura, S., and Wang, J. 2019. A simple framework for describing strength of saturated frozen soils as multi-phase coupled system. Geotechnique, **69**(8): 659–671. doi:10.1680/jgeot.17.P.104.

Nishimura, S., Gens, A., Olivella, S., and Jardine, R.J. 2009. THM-coupled finite element analysis of frozen soil: Formulation and application. Geotechnique, **59**(3): 159–171. doi:10.1680/geot.2009.59.3.159.

Reiffsteck, P., Nguyen Pham, P.T., and Arbaut, J. 2007. Influence of particle size distribution on the mechanical behavior of a soil. Bulletin de Liaison des Laboratoires des Ponts et Chaussées, Paris, France.

Ren, X.W., and Santamarina, J.C. 2018. The hydraulic conductivity of sediments: a pore size perspective. Engineering Geology, **233**(November 2017): 48–54. doi:10.1016/j.enggeo.2017.11.022.

Romero, E. 2013. A microstructural insight into compacted clayey soils and their hydraulic properties. Engineering Geology, **165**: 3–19. doi:10.1016/j.enggeo.2013.05.024.

Shuplik, M., and Nikolaev, P. 2019. Advanced ground freezing method and its applications in underground construction. MATEC Web of Conferences, **265**: 04021. doi:10.1051/matecconf/201926504021.

Taber, S. 1930. The mechanics of frost heaving. Journal of Geology, **38**(4): 303–317.

Van Genuchten, M.T. 1980. A closed-form equation for predicting the hydraulic conductivity of unsaturated soils. Soil Science Society of America Journal, **44**(5): 892–898.

Viggiani, G., and Casini, F. 2015. Artificial ground freezing: from applications and case studies to fundamental research. *In* Geotechnical engineering for infrastructure and development—Proceedings of the XVI European Conference on Soil Mechanics and Geotechnical Engineering, ECSMGE 2015. pp. 65–92. ICE Publishing, London, UK. doi:10.1680/ecsmge.60678.

Viggiani, G., and De Sanctis, L. 2009. Geotechnical aspects of underground railway construction in the urban environment: the examples of Rome and Naples. Geological Society Engineering Geology Special Publication, **22**(1): 215–240. doi:10.1144/EGSP22.18.

Vu, Q.H. 2022. Effect of fines content on hydro-thermal behaviour of sandy soil in the context of artificial ground freezing. Ph.D. thesis, Ecole des Ponts ParisTech, Paris, France.

Vu, Q.H., Pereira, J.M., and Tang, A.M. 2022. Effect of fines content on soil freezing characteristic curve of sandy soils. Acta Geotechnica, **17**(11): 4921–4933. doi:10.1007/s11440-022-01672-9.

Wang, C., Lai, Y., and Zhang, M. 2017. Estimating soil freezing characteristic curve based on pore-size distribution. Applied Thermal Engineering, **124**: 1049–1060.

Wang, H., Wu, Y., Wang, M., and Li, X. 2022. Influence of fines content and degree of saturation on the freezing deformation characteristics of unsaturated soils. Cold Regions Science and Technology, **201**:103610. doi:10.1016/j.coldregions.2022.103610.

Wang, H., Vanapalli, S.K., and Li, X. 2025. A unified model for the soil freezing characteristic curve based on pore size distribution and principles of thermodynamics. Water Resources Research, **61**(3): e2024WR038715.

Wettlaufer, J., and Worster, M.G. 2006. Premelting dynamics. Annual Review of Financial Economics, **38**(1): 427–452. doi:10.1146/annurev.fluid.37.061903.175758.

Xu, X., Li, Q., Lai, Y., Pang, W., and Zhang, R. 2019. Effect of moisture content on mechanical and damage behavior of frozen loess under triaxial condition along with different confining pressures. Cold Regions Science and Technology, **157**(2018): 110–118. doi:10.1016/j.coldregions.2018.10.004.

Yamamoto, Y., and Springman, S.M. 2014. Axial compression stress path tests on artificial frozen soil samples in a triaxial device at temperatures just below 0 °C. Canadian Geotechnical Journal, **51**(10): 1178–1195. doi:10.1139/cgj-2013-0257.

Yang, N., Zheng, H., Cai, H., Liu, Y., and Nishimura, S. 2024. Study on multidimensional frost heave characteristics and thermal-hydro-mechanical predictive model. Cold Regions Science and Technology, **224**: 104227.

Yang, S., Lacasse, S., and Sandven, R. 2006. Determination of the transitional fines content of mixtures of sand and non-plastic fines. Geotechnical Testing Journal, **29**(2): 102–107. doi:10.1520/GTJ14010.

Yin, K., Fauchille, A.L., Di Filippo, E., Kotronis, P., and Sciarra, G. 2021. A review of sand–clay mixture and soil–structure interface direct shear test. Geotechnics, **1**(2): 260–306. doi:10.3390/geotechnics1020014.

Zhou, J., Wei, C., Wei, H., and Tan, L. 2014. Experimental and theoretical characterization of frost heave and ice lenses. Cold Regions Science and Technology, **104–105**: 76–87. doi:10.1016/j.coldregions.2014.05.002.